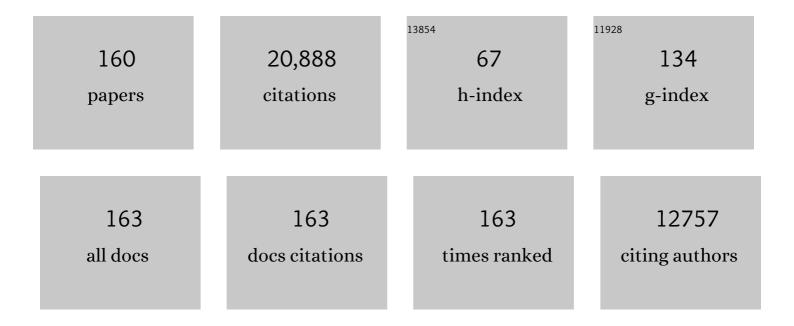
## Pablo J Zarco-Tejada

List of Publications by Year in descending order

Source: https://exaly.com/author-pdf/7867196/publications.pdf Version: 2024-02-01



#	Article	IF	CITATIONS
1	Residual Effect and N Fertilizer Rate Detection by High-Resolution VNIR-SWIR Hyperspectral Imagery and Solar-Induced Chlorophyll Fluorescence in Wheat. IEEE Transactions on Geoscience and Remote Sensing, 2022, 60, 1-17.	2.7	18
2	Evaluation of SIF retrievals from narrow-band and sub-nanometer airborne hyperspectral imagers flown in tandem: Modelling and validation in the context of plant phenotyping. Remote Sensing of Environment, 2022, 273, 112986.	4.6	15
3	Assessment of peach trees water status and leaf gas exchange using on-the-ground versus airborne-based thermal imagery. Agricultural Water Management, 2022, 267, 107628.	2.4	5
4	Evaluating the role of solar-induced fluorescence (SIF) and plant physiological traits for leaf nitrogen assessment in almond using airborne hyperspectral imagery. Remote Sensing of Environment, 2022, 279, 113141.	4.6	13
5	High-Throughput Estimation of Crop Traits: A Review of Ground and Aerial Phenotyping Platforms. IEEE Geoscience and Remote Sensing Magazine, 2021, 9, 200-231.	4.9	141
6	Assessing the contribution of understory sun-induced chlorophyll fluorescence through 3-D radiative transfer modelling and field data. Remote Sensing of Environment, 2021, 253, 112195.	4.6	22
7	Normalization of the crop water stress index to assess the within-field spatial variability of water stress sensitivity. Precision Agriculture, 2021, 22, 964-983.	3.1	9
8	Physical model inversion of the green spectral region to track assimilation rate in almond trees with an airborne nano-hyperspectral imager. Remote Sensing of Environment, 2021, 252, 112147.	4.6	11
9	Assessment of Satellite Chlorophyll-Based Leaf Maximum Carboxylation Rate (Vcmax) Using Flux Observations at Crop and Grass Sites. IEEE Journal of Selected Topics in Applied Earth Observations and Remote Sensing, 2021, 14, 5352-5360.	2.3	3
10	38. Integrating vegetation vigour in a thermal sensitivity index for mapping the variability of orchard water stress. , 2021, , .		0
11	Using an unmanned platform and VIS-NIR cameras to determine biophysical and geometrical parameters of olive, grapevine and citrus canopies. Acta Horticulturae, 2021, , 345-352.	0.1	1
12	Detection of Xylella fastidiosa in almond orchards by synergic use of an epidemic spread model and remotely sensed plant traits. Remote Sensing of Environment, 2021, 260, 112420.	4.6	24
13	Simultaneous assessment of nitrogen and water status in winter wheat using hyperspectral and thermal sensors. European Journal of Agronomy, 2021, 127, 126287.	1.9	21
14	Assessing wine grape quality parameters using plant traits derived from physical model inversion of hyperspectral imagery. Agricultural and Forest Meteorology, 2021, 306, 108445.	1.9	9
15	Discriminating Xylella fastidiosa from Verticillium dahliae infections in olive trees using thermal- and hyperspectral-based plant traits. ISPRS Journal of Photogrammetry and Remote Sensing, 2021, 179, 133-144.	4.9	29
16	Modelling hyperspectral- and thermal-based plant traits for the early detection of Phytophthora-induced symptoms in oak decline. Remote Sensing of Environment, 2021, 263, 112570.	4.6	32
17	Long-term effects of water stress on hyperspectral remote sensing indicators in young radiata pine. Forest Ecology and Management, 2021, 502, 119707.	1.4	11
18	Comparing the Retrieval of Chlorophyll Fluorescence from Two Airborne Hyperspectral Imagers with Different Spectral Resolutions for Plant Phenotyping Studies. , 2021, , .		1

#	Article	IF	CITATIONS
19	Divergent abiotic spectral pathways unravel pathogen stress signals across species. Nature Communications, 2021, 12, 6088.	5.8	40
20	Monitoring the incidence of Xylella fastidiosa infection in olive orchards using ground-based evaluations, airborne imaging spectroscopy and Sentinel-2 time series through 3-D radiative transfer modelling. Remote Sensing of Environment, 2020, 236, 111480.	4.6	49
21	Using hyperspectral plant traits linked to photosynthetic efficiency to assess N and P partition. ISPRS Journal of Photogrammetry and Remote Sensing, 2020, 169, 406-420.	4.9	19
22	Monitoring biochemical limitations to photosynthesis in N and P-limited radiata pine using plant functional traits quantified from hyperspectral imagery. Remote Sensing of Environment, 2020, 248, 112003.	4.6	16
23	Empirical validation of the relationship between the crop water stress index and relative transpiration in almond trees. Agricultural and Forest Meteorology, 2020, 292-293, 108128.	1.9	11
24	A Heritage Science Workflow to Preserve and Narrate a Rural Archeological Landscape Using Virtual Reality: The Cerro del Castillo of Belmez and Its Surrounding Environment (Cordoba, Spain). Applied Sciences (Switzerland), 2020, 10, 8659.	1.3	11
25	Detection of Xylella fastidiosa infection symptoms with airborne multispectral and thermal imagery: Assessing bandset reduction performance from hyperspectral analysis. ISPRS Journal of Photogrammetry and Remote Sensing, 2020, 162, 27-40.	4.9	55
26	Spaceborne Imaging Spectroscopy for Sustainable Agriculture: Contributions and Challenges. Surveys in Geophysics, 2019, 40, 515-551.	2.1	85
27	Breaking down barriers between remote sensing and plant pathology. Tropical Plant Pathology, 2019, 44, 398-400.	0.8	13
28	Remote sensing of solar-induced chlorophyll fluorescence (SIF) in vegetation: 50†years of progress. Remote Sensing of Environment, 2019, 231, 111177.	4.6	372
29	Unmanned Aerial System multispectral mapping for low and variable solar irradiance conditions: Potential of tensor decomposition. ISPRS Journal of Photogrammetry and Remote Sensing, 2019, 155, 58-71.	4.9	28
30	Early Diagnosis of Vegetation Health From High-Resolution Hyperspectral and Thermal Imagery: Lessons Learned From Empirical Relationships and Radiative Transfer Modelling. Current Forestry Reports, 2019, 5, 169-183.	3.4	58
31	High-resolution imagery acquired from an unmanned platform to estimate biophysical and geometrical parameters of olive trees under different irrigation regimes. PLoS ONE, 2019, 14, e0210804.	1.1	60
32	Chlorophyll content estimation in an open-canopy conifer forest with Sentinel-2A and hyperspectral imagery in the context of forest decline. Remote Sensing of Environment, 2019, 223, 320-335.	4.6	112
33	Advantages of retrieving pigment content [î¼g/cm2] versus concentration [%] from canopy reflectance. Remote Sensing of Environment, 2019, 230, 111195.	4.6	38
34	Radiative transfer Vcmax estimation from hyperspectral imagery and SIF retrievals to assess photosynthetic performance in rainfed and irrigated plant phenotyping trials. Remote Sensing of Environment, 2019, 231, 111186.	4.6	61
35	High spatial resolution monitoring land surface energy, water and CO2 fluxes from an Unmanned Aerial System. Remote Sensing of Environment, 2019, 229, 14-31.	4.6	43
36	Genetic dissection of agronomic and quality traits based on association mapping and genomic selection approaches in durum wheat grown in Southern Spain. PLoS ONE, 2019, 14, e0211718.	1.1	29

#	Article	IF	CITATIONS
37	Transpiration from canopy temperature: Implications for the assessment of crop yield in almond orchards. European Journal of Agronomy, 2019, 105, 78-85.	1.9	32
38	Impact of the spatial resolution on the energy balance components on an open-canopy olive orchard. International Journal of Applied Earth Observation and Geoinformation, 2019, 74, 88-102.	1.4	27
39	Hotspots in the genomic architecture of field drought responses in wheat as breeding targets. Functional and Integrative Genomics, 2019, 19, 295-309.	1.4	40
40	Understanding the temporal dimension of the red-edge spectral region for forest decline detection using high-resolution hyperspectral and Sentinel-2a imagery. ISPRS Journal of Photogrammetry and Remote Sensing, 2018, 137, 134-148.	4.9	71
41	Maximizing the relationship of yield to site-specific management zones with object-oriented segmentation of hyperspectral images. Precision Agriculture, 2018, 19, 348-364.	3.1	11
42	Evaluating the performance of xanthophyll, chlorophyll and structure-sensitive spectral indices to detect water stress in five fruit tree species. Precision Agriculture, 2018, 19, 178-193.	3.1	58
43	Assessment of the Spatial Varability of CWSI Within Almond Tree Crowns and its Effects on the Relationship with Stomatal Conductance. , 2018, , .		1
44	Monitoring Forest Health with Sun-Induced Chlorophyll Fluorescence Observations and 3-D Radiative Transfer Modeling. , 2018, , .		0
45	Using Sentinel-2 Imagery to Track Changes Produced by Xylella Fastidiosa in Olive Trees. , 2018, , .		3
46	Effects of Heterogeneity within Tree Crowns on Airborne-Quantified SIF and the CWSI as Indicators of Water Stress in the Context of Precision Agriculture. Remote Sensing, 2018, 10, 604.	1.8	32
47	Multi-Temporal and Spectral Analysis of High-Resolution Hyperspectral Airborne Imagery for Precision Agriculture: Assessment of Wheat Grain Yield and Grain Protein Content. Remote Sensing, 2018, 10, 930.	1.8	41
48	Previsual symptoms of Xylella fastidiosa infection revealed in spectral plant-trait alterations. Nature Plants, 2018, 4, 432-439.	4.7	212
49	Quantitative Remote Sensing at Ultra-High Resolution with UAV Spectroscopy: A Review of Sensor Technology, Measurement Procedures, and Data Correction Workflows. Remote Sensing, 2018, 10, 1091.	1.8	375
50	Improved nitrogen retrievals with airborne-derived fluorescence and plant traits quantified from VNIR-SWIR hyperspectral imagery in the context of precision agriculture. International Journal of Applied Earth Observation and Geoinformation, 2018, 70, 105-117.	1.4	67
51	Assessing the effects of forest health on sun-induced chlorophyll fluorescence using the FluorFLIGHT 3-D radiative transfer model to account for forest structure. Remote Sensing of Environment, 2017, 193, 165-179.	4.6	94
52	Airborne and ground level sensors for monitoring nitrogen status in a maize crop. Biosystems Engineering, 2017, 160, 124-133.	1.9	80
53	Spatio-Temporal Relationships between Optical Information and Carbon Fluxes in a Mediterranean Tree-Grass Ecosystem. Remote Sensing, 2017, 9, 608.	1.8	15
54	Tree crown parameters assessment using 3D photo reconstruction as a tool for selection in olive breeding programs. Acta Horticulturae, 2017, , 1-4.	0.1	3

#	Article	IF	CITATIONS
55	Estimating evaporation with thermal UAV data and two-source energy balance models. Hydrology and Earth System Sciences, 2016, 20, 697-713.	1.9	119
56	Airborne Thermal Imagery to Detect the Seasonal Evolution of Crop Water Status in Peach, Nectarine and Saturn Peach Orchards. Remote Sensing, 2016, 8, 39.	1.8	83
57	Early Detection and Quantification of Almond Red Leaf Blotch Using High-Resolution Hyperspectral and Thermal Imagery. Remote Sensing, 2016, 8, 276.	1.8	90
58	A Novel Remote Sensing Approach for Prediction of Maize Yield Under Different Conditions of Nitrogen Fertilization. Frontiers in Plant Science, 2016, 7, 666.	1.7	98
59	Vineyard irrigation scheduling based on airborne thermal imagery and water potential thresholds. Australian Journal of Grape and Wine Research, 2016, 22, 307-315.	1.0	88
60	Seasonal stability of chlorophyll fluorescence quantified from airborne hyperspectral imagery as an indicator of net photosynthesis in the context of precision agriculture. Remote Sensing of Environment, 2016, 179, 89-103.	4.6	112
61	High-Resolution Airborne UAV Imagery to Assess Olive Tree Crown Parameters Using 3D Photo Reconstruction: Application in Breeding Trials. Remote Sensing, 2015, 7, 4213-4232.	1.8	263
62	Early Detection and Quantification of Verticillium Wilt in Olive Using Hyperspectral and Thermal Imagery over Large Areas. Remote Sensing, 2015, 7, 5584-5610.	1.8	162
63	Using High-Resolution Hyperspectral and Thermal Airborne Imagery to Assess Physiological Condition in the Context of Wheat Phenotyping. Remote Sensing, 2015, 7, 13586-13605.	1.8	75
64	Unmanned aerial platform-based multi-spectral imaging for field phenotyping of maize. Plant Methods, 2015, 11, 35.	1.9	248
65	Seasonal evolution of crop water stress index in grapevine varieties determined with high-resolution remote sensing thermal imagery. Irrigation Science, 2015, 33, 81-93.	1.3	102
66	Improving the precision of irrigation in a pistachio farm using an unmanned airborne thermal system. Irrigation Science, 2015, 33, 43-52.	1.3	55
67	High resolution remote and proximal sensing to assess low and high yield areas in a wheat field. , 2015, , 191-198.		3
68	Soil Temperature Determines the Reaction of Olive Cultivars to Verticillium dahliae Pathotypes. PLoS ONE, 2014, 9, e110664.	1.1	34
69	A Novel Methodology to Estimate Single-Tree Biophysical Parameters from 3D Digital Imagery Compared to Aerial Laser Scanner Data. Remote Sensing, 2014, 6, 11627-11648.	1.8	34
70	Deriving Predictive Relationships of Carotenoid Content at the Canopy Level in a Conifer Forest Using Hyperspectral Imagery and Model Simulation. IEEE Transactions on Geoscience and Remote Sensing, 2014, 52, 5206-5217.	2.7	27
71	Estimating Radiation Interception in Heterogeneous Orchards Using High Spatial Resolution Airborne Imagery. IEEE Geoscience and Remote Sensing Letters, 2014, 11, 579-583.	1.4	13
72	Reply to Magnani et al.: Linking large-scale chlorophyll fluorescence observations with cropland gross primary production. Proceedings of the National Academy of Sciences of the United States of America, 2014, 111, E2511.	3.3	11

#	Article	IF	CITATIONS
73	Mapping crop water stress index in a â€~Pinot-noir' vineyard: comparing ground measurements with thermal remote sensing imagery from an unmanned aerial vehicle. Precision Agriculture, 2014, 15, 361-376.	3.1	261
74	The normalized topographic method: an automated procedure for gully mapping using GIS. Earth Surface Processes and Landforms, 2014, 39, 2002-2015.	1.2	55
75	Global and time-resolved monitoring of crop photosynthesis with chlorophyll fluorescence. Proceedings of the National Academy of Sciences of the United States of America, 2014, 111, E1327-33.	3.3	741
76	Unmixing-Based Fusion of Hyperspatial and Hyperspectral Airborne Imagery for Early Detection of Vegetation Stress. IEEE Journal of Selected Topics in Applied Earth Observations and Remote Sensing, 2014, 7, 2571-2582.	2.3	42
77	Applicability and limitations of using the crop water stress index as an indicator of water deficits in citrus orchards. Agricultural and Forest Meteorology, 2014, 198-199, 94-104.	1.9	122
78	Detection of downy mildew of opium poppy using high-resolution multi-spectral and thermal imagery acquired with an unmanned aerial vehicle. Precision Agriculture, 2014, 15, 639-661.	3.1	57
79	Automatic identification of agricultural terraces through object-oriented analysis of very high resolution DSMs and multispectral imagery obtained from an unmanned aerial vehicle. Journal of Environmental Management, 2014, 134, 117-126.	3.8	91
80	Tree height quantification using very high resolution imagery acquired from an unmanned aerial vehicle (UAV) and automatic 3D photo-reconstruction methods. European Journal of Agronomy, 2014, 55, 89-99.	1.9	426
81	Airborne Hyperspectral Images and Ground-Level Optical Sensors As Assessment Tools for Maize Nitrogen Fertilization. Remote Sensing, 2014, 6, 2940-2962.	1.8	114
82	A tool for detecting crop water status using airborne high-resolution thermal imagery. , 2014, , .		3
83	Using high resolution UAV thermal imagery to assess the variability in the water status of five fruit tree species within a commercial orchard. Precision Agriculture, 2013, 14, 660-678.	3.1	255
84	Retrieval of biophysical vegetation parameters using simultaneous inversion of high resolution remote sensing imagery constrained by a vegetation index. Precision Agriculture, 2013, 14, 541-557.	3.1	7
85	High-resolution airborne hyperspectral and thermal imagery for early detection of Verticillium wilt of olive using fluorescence, temperature and narrow-band spectral indices. Remote Sensing of Environment, 2013, 139, 231-245.	4.6	354
86	A PRI-based water stress index combining structural and chlorophyll effects: Assessment using diurnal narrow-band airborne imagery and the CWSI thermal index. Remote Sensing of Environment, 2013, 138, 38-50.	4.6	237
87	Using radiometric surface temperature for surface energy flux estimation in Mediterranean drylands from a two-source perspective. Remote Sensing of Environment, 2013, 136, 234-246.	4.6	59
88	Estimating leaf carotenoid content in vineyards using high resolution hyperspectral imagery acquired from an unmanned aerial vehicle (UAV). Agricultural and Forest Meteorology, 2013, 171-172, 281-294.	1.9	228
89	Spatio-temporal patterns of chlorophyll fluorescence and physiological and structural indices acquired from hyperspectral imagery as compared with carbon fluxes measured with eddy covariance. Remote Sensing of Environment, 2013, 133, 102-115.	4.6	164
90	Relationships between net photosynthesis and steady-state chlorophyll fluorescence retrieved from airborne hyperspectral imagery. Remote Sensing of Environment, 2013, 136, 247-258.	4.6	130

#	Article	IF	CITATIONS
91	Spatial Resolution Effects on Chlorophyll Fluorescence Retrieval in a Heterogeneous Canopy Using Hyperspectral Imagery and Radiative Transfer Simulation. IEEE Geoscience and Remote Sensing Letters, 2013, 10, 937-941.	1.4	48
92	Estimating radiation interception in an olive orchard using physical models and multispectral airborne imagery. Israel Journal of Plant Sciences, 2012, 60, 107-121.	0.3	11
93	THE PHOTOCHEMICAL REFLECTANCE INDEX (PRI) AS A WATER STRESS INDICATOR IN PEACH ORCHARDS FROM REMOTE SENSING IMAGERY. Acta Horticulturae, 2012, , 363-369.	0.1	2
94	RESPONSES OF NECTARINE TO REGULATED DEFICIT IRRIGATION AT THE FIELD SCALE. Acta Horticulturae, 2012, , 349-353.	0.1	0
95	REMOTE SENSING OF THERMAL WATER STRESS INDICATORS IN PEACH. Acta Horticulturae, 2012, , 325-331.	0.1	5
96	Fluorescence, temperature and narrow-band indices acquired from a UAV platform for water stress detection using a micro-hyperspectral imager and a thermal camera. Remote Sensing of Environment, 2012, 117, 322-337.	4.6	747
97	Almond tree canopy temperature reveals intra-crown variability that is water stress-dependent. Agricultural and Forest Meteorology, 2012, 154-155, 156-165.	1.9	107
98	Monitoring water stress and fruit quality in an orange orchard under regulated deficit irrigation using narrow-band structural and physiological remote sensing indices. ISPRS Journal of Photogrammetry and Remote Sensing, 2012, 71, 47-61.	4.9	107
99	Carotenoid content estimation in a heterogeneous conifer forest using narrow-band indices and PROSPECT + DART simulations. Remote Sensing of Environment, 2012, 127, 298-315.	4.6	117
100	Mapping radiation interception in row-structured orchards using 3D simulation and high-resolution airborne imagery acquired from a UAV. Precision Agriculture, 2012, 13, 473-500.	3.1	62
101	Field characterization of olive (Olea europaea L.) tree crown architecture using terrestrial laser scanning data. Agricultural and Forest Meteorology, 2011, 151, 204-214.	1.9	132
102	Determining Biophysical Parameters for Olive Trees Using CASIâ€Airborne and Quickbird‣atellite Imagery. Agronomy Journal, 2011, 103, 644-654.	0.9	30
103	ORCHARD WATER STRESS DETECTION USING HIGH-RESOLUTION IMAGERY. Acta Horticulturae, 2011, , 35-39.	0.1	3
104	Assessing structural effects on PRI for stress detection in conifer forests. Remote Sensing of Environment, 2011, 115, 2360-2375.	4.6	209
105	RESPONSE TO REGULATED DEFICIT IRRIGATION OF A NECTARINE ORCHARD IN SOUTHERN SPAIN. Acta Horticulturae, 2011, , 217-220.	0.1	0
106	Detecting water stress effects on fruit quality in orchards with time-series PRI airborne imagery. Remote Sensing of Environment, 2010, 114, 286-298.	4.6	107
107	Grape quality assessment in vineyards affected by iron deficiency chlorosis using narrow-band physiological remote sensing indices. Remote Sensing of Environment, 2010, 114, 1968-1986.	4.6	98
108	Thermal and Narrowband Multispectral Remote Sensing for Vegetation Monitoring From an Unmanned Aerial Vehicle. IEEE Transactions on Geoscience and Remote Sensing, 2009, 47, 722-738.	2.7	972

#	Article	IF	CITATIONS
109	Retrieval of foliar information about plant pigment systems from high resolution spectroscopy. Remote Sensing of Environment, 2009, 113, S67-S77.	4.6	576
110	Modelling PRI for water stress detection using radiative transfer models. Remote Sensing of Environment, 2009, 113, 730-744.	4.6	116
111	Imaging chlorophyll fluorescence with an airborne narrow-band multispectral camera for vegetation stress detection. Remote Sensing of Environment, 2009, 113, 1262-1275.	4.6	242
112	PROSPECT+SAIL models: A review of use for vegetation characterization. Remote Sensing of Environment, 2009, 113, S56-S66.	4.6	1,178
113	Mapping canopy conductance and CWSI in olive orchards using high resolution thermal remote sensing imagery. Remote Sensing of Environment, 2009, 113, 2380-2388.	4.6	314
114	Discriminating irrigated and rainfed olive orchards with thermal ASTER imagery and DART 3D simulation. Agricultural and Forest Meteorology, 2009, 149, 962-975.	1.9	36
115	Thermal remote sensing from Airborne Hyperspectral Scanner data in the framework of the SPARC and SEN2FLEX projects: an overview. Hydrology and Earth System Sciences, 2009, 13, 2031-2037.	1.9	25
116	Assessing canopy PRI for water stress detection with diurnal airborne imagery. Remote Sensing of Environment, 2008, 112, 560-575.	4.6	224
117	Model inversion for chlorophyll estimation in open canopies from hyperspectral imagery. International Journal of Remote Sensing, 2008, 29, 5093-5111.	1.3	30
118	Boreal forest mapping at the BOREAS study area using seasonal optical indices sensitive to plant pigment content. Canadian Journal of Remote Sensing, 2008, 34, S158-S171.	1.1	7
119	A new era in remote sensing of crops with unmanned robots. SPIE Newsroom, 2008, , .	0.1	37
120	Detecting crop irrigation status in orchard canopies with airborne and ASTER thermal imagery. , 2007, , $\cdot$		0
121	Surface temperature in the context of FLuorescence EXplorer (FLEX) mission. , 2007, , .		0
122	Relationships between Moderate Resolution Imaging Spectroradiometer water indexes and tower flux data in an old growth conifer forest. Journal of Applied Remote Sensing, 2007, 1, 013513.	0.6	12
123	Estimation of evapotranspiration on discontinuous crop canopies using high resolution thermal imagery. , 2007, , .		1
124	Extracting tree crown properties from ground-based scanning laser data. , 2007, , .		3
125	Monitoring yield and fruit quality parameters in open-canopy tree crops under water stress. Implications for ASTER. Remote Sensing of Environment, 2007, 107, 455-470.	4.6	73
126	Detection of water stress in an olive orchard with thermal remote sensing imagery. Agricultural and Forest Meteorology, 2006, 136, 31-44.	1.9	186

#	Article	IF	CITATIONS
127	Stress detection in orchards with hyperspectral remote sensing data. , 2006, 6359, 240.		1
128	Land surface temperature derived from airborne hyperspectral scanner thermal infrared data. Remote Sensing of Environment, 2006, 102, 99-115.	4.6	104
129	Estimating vegetation water content with hyperspectral data for different canopy scenarios: Relationships between AVIRIS and MODIS indexes. Remote Sensing of Environment, 2006, 105, 354-366.	4.6	146
130	FluorMODgui V3.0: A graphic user interface for the spectral simulation of leaf and canopy chlorophyll fluorescence. Computers and Geosciences, 2006, 32, 577-591.	2.0	36
131	Hyperspectral mapping of crop and soils for precision agriculture. , 2006, 6298, 84.		17
132	Canopy water content estimates with AVIRIS imagery and MODIS reflectance products. , 2006, , .		1
133	Retrieval of Quantitative and Qualitative Information about Plant Pigment Systems from High Resolution Spectroscopy. , 2006, , .		6
134	PROSPECT+SAIL: 15 Years of Use for Land Surface Characterization. , 2006, , .		9
135	Simple reflectance indices track heat and water stress-induced changes in steady-state chlorophyll fluorescence at the canopy scale. Remote Sensing of Environment, 2005, 97, 403-414.	4.6	259
136	Assessing vineyard condition with hyperspectral indices: Leaf and canopy reflectance simulation in a row-structured discontinuous canopy. Remote Sensing of Environment, 2005, 99, 271-287.	4.6	589
137	Estimation of fuel moisture content by inversion of radiative transfer models to simulate equivalent water thickness and dry matter content: analysis at leaf and canopy level. IEEE Transactions on Geoscience and Remote Sensing, 2005, 43, 819-826.	2.7	175
138	Detection of water stress in orchard trees with a high-resolution spectrometer through chlorophyll fluorescence in-filling of the O/sub 2/-A band. IEEE Transactions on Geoscience and Remote Sensing, 2005, 43, 2860-2869.	2.7	94
139	Temporal and Spatial Relationships between Within-Field Yield Variability in Cotton and High-Spatial Hyperspectral Remote Sensing Imagery. Agronomy Journal, 2005, 97, 641-653.	0.9	189
140	Needle chlorophyll content estimation through model inversion using hyperspectral data from boreal conifer forest canopies. Remote Sensing of Environment, 2004, 89, 189-199.	4.6	174
141	Remote sensing in BOREAS: Lessons learned. Remote Sensing of Environment, 2004, 89, 139-162.	4.6	76
142	Hyperspectral vegetation indices and novel algorithms for predicting green LAI of crop canopies: Modeling and validation in the context of precision agriculture. Remote Sensing of Environment, 2004, 90, 337-352.	4.6	1,819
143	Hyperspectral indices and model simulation for chlorophyll estimation in open-canopy tree crops. Remote Sensing of Environment, 2004, 90, 463-476.	4.6	332
144	Water content estimation in vegetation with MODIS reflectance data and model inversion methods. Remote Sensing of Environment, 2003, 85, 109-124.	4.6	450

#	Article	IF	CITATIONS
145	Steady-state chlorophyll a fluorescence detection from canopy derivative reflectance and double-peak red-edge effects. Remote Sensing of Environment, 2003, 84, 283-294.	4.6	297
146	Vegetation Stress Detection through Chlorophyll <i>a</i> + <i>b</i> Estimation and Fluorescence Effects on Hyperspectral Imagery. Journal of Environmental Quality, 2002, 31, 1433-1441.	1.0	229
147	Integrated narrow-band vegetation indices for prediction of crop chlorophyll content for application to precision agriculture. Remote Sensing of Environment, 2002, 81, 416-426.	4.6	1,379
148	Remote Sensing of Solar-Induced Chlorophyll Fluorescence from Vegetation Hyperspectral Reflectance and Radiative Transfer Simulation. , 2002, , 233-269.		3
149	Scaling-up and model inversion methods with narrowband optical indices for chlorophyll content estimation in closed forest canopies with hyperspectral data. IEEE Transactions on Geoscience and Remote Sensing, 2001, 39, 1491-1507.	2.7	529
150	Estimation of chlorophyll fluorescence under natural illumination from hyperspectral data. International Journal of Applied Earth Observation and Geoinformation, 2001, 3, 321-327.	1.4	45
151	Chlorophyll Fluorescence Effects on Vegetation Apparent Reflectance I. Leaf-Level Measurements and Model Simulation. Remote Sensing of Environment, 2000, 74, 582-595.	4.6	221
152	Chlorophyll Fluorescence Effects on Vegetation Apparent Reflectance II. Laboratory and Airborne Canopy-Level Measurements with Hyperspectral Data. Remote Sensing of Environment, 2000, 74, 596-608.	4.6	125
153	The Bioindicators of Forest Condition Project: A physiological, remote sensing approach. Forestry Chronicle, 2000, 76, 941-952.	0.5	26
154	Land cover mapping at BOREAS using red edge spectral parameters from CASI imagery. Journal of Geophysical Research, 1999, 104, 27921-27933.	3.3	88
155	Canopy optical indices from infinite reflectance and canopy reflectance models for forest condition monitoring: application to hyperspectral CASI data. , 0, , .		11
156	Minimization of shadow effects in forest canopies for chlorophyll content estimation using red edge optical indices through radiative transfer: implications for MERIS. , 0, , .		0
157	Modeling canopy water content for carbon estimates from MODIS data at land EOS validation sites. , 0, , .		29
158	Using support vector machines to automatically extract open water signatures from POLDER multi-angle data over boreal regions. , 0, , .		1
159	Chlorophyll content estimation of Boreal conifers using hyperspectral remote sensing. , 0, , .		4
160	Progress on the development of an integrated canopy fluorescence model. , 0, , .		9